PCCP

External electric field effect on the lowest excited states of indole: *ab initio* and molecular dynamics study

C. Dedonder-Lardeux,[a] C. Jouvet,[a] S. Perun[b] and A. L. Sobolewski[b]

[a] *Laboratoire de Photophysique Moléculaire du CNRS, Université Paris-Sud, Bât. 210, F-91405, Orsay Cedex, France. E-mail: claude.dedonder-lardeaux@ppm.u-psud.fr*
[b] *Institute of Physics, Polish Academy of Sciences, PL-02668, Warsaw, Poland*

Received 29th July 2003, Accepted 19th September 2003
First published as an Advance Article on the web 9th October 2003

The external electric field effect on the lowest excited states of indole was studied with the aid of second-order Møller–Plesset perturbation theory based on the complete-active-space self-consistent-field wave function (CASMP2) and the time-dependent density functional theory (TDDFT) methods. The order of magnitude of the electric field experienced by indole in water and by the indole chromophore of tryptophan within a protein in aqueous environment was estimated using molecular dynamics simulations with the Amber force field. It has been shown that, at 300 K, the magnitude of the field is fluctuating significantly up to 5×10^{-3} a.u. The CASMP2 and TDDFT energy of the lowest $\pi\pi^*$ singlet state (L_b) shows only a relatively small variation within the limit of the applied field, but the next $\pi\pi^*$ singlet state (L_a) and the lowest $\pi\sigma^*$ singlet state of Rydberg character are strongly influenced by the field, and for $|E| \cong 5 \times 10^{-3}$ a.u. either the strongly emitting $L_a(\pi\pi^*)$ state or the essentially "dark" $\pi\sigma^*$ state (depending on the orientation of the electric field vector) becomes the lowest excited singlet state of the system. Since the lifetime of the emitting singlet state is governed by the $\pi\pi^*/\pi\sigma^*$ crossing, as demonstrated in many experiments in clusters, this local field effect provides an attractive mechanistic picture for understanding the variations of the tryptophan fluorescence lifetime in proteins.

1 Introduction

The electronically excited states of indole and substituted indoles have attracted considerable attention in the context of understanding the complex photophysical behavior of tryptophan (Trp) side chains in proteins. The Trp fluorescence is highly sensitive to the environment, making it an ideal choice for reporting protein conformation changes and interactions with other molecules.[1] The properties used are changes in fluorescence intensity, wavelength maximum (λ_{max}), band shape, anisotropy and fluorescence lifetime. The power of this probe has been considerably amplified since Trp can often be substituted for other amino acids, by site-directed mutagenesis, with minimal effect on structure and activity. The emission spectrum of Trp in proteins varies from a structured band to a broad, diffuse band with wavelength maximum spanning a 40-nm range. The fluorescence quantum yield ranges from 0.35 to near zero.[2]

The environmental sensitivity of the wavelength of the emission maximum seems to be well understood.[3] It has been clearly shown that the shifts are due to the electric field imposed by the protein and the solvent on the indole chromophore of Trp. This may be termed as an *internal* Stark effect, by analogy to the familiar shifting of energy levels *via* an applied (external) field. The agreement of prediction and experimental observations presented in ref. 3 seems to be very good, so one can assume that the local electric field direction and magnitude determine primarily the sign and magnitude of the fluorescence shifts relative to vacuum. The relative orientation and intensity of the electric field at the indole ring determines whether there will be a red shift, a blue shift, or no shift at all.

The variation of the Trp fluorescence lifetime or of its indole chromophore has also been the subject of many investigations in both the condensed and gas phases.[1,4–16] However, no clear picture emerges from these works that allows to understand why the fluorescence lifetime (or the fluorescence quantum yield) is varying by more than two orders of magnitude, depending on the environment. To account for this effect, the existence of very fast non-radiative decay channels that efficiently quench the fluorescence is anticipated. The non-radiative processes which determine the lifetime of the excited states are presumably ultrafast internal conversion back to the electronic ground state[8] and photoionization (formation of solvated electrons) in aqueous solution.[6,12] In the gas phase, numerous papers have discussed the role of the L_a–L_b inversion,[8,11,13] the L_a state being thought to be responsible for the short lifetime of indole, but both experiments[5] and calculations[17] give similar (within a factor of three) radiative lifetimes for these two states. Thus, the L_a–L_b inversion mechanism does not explain how the lifetime of the excited state can vary by more than two orders of magnitude.

In water solution, Trp exhibits a dual lifetime with $\tau_1 = 0.3$ ns and $\tau_2 = 3$ ns depending on the temperature and pH.[1] These two components have been assigned to two rotamers, linked to the positions of the protonated amino group (NH_3^+) and the ionized carboxy (CO_2^-) group *versus* the indole ring. The variations of the lifetime itself have been explained either by a proton transfer or by an electron transfer mechanism.[7]

Many single-Trp proteins also display double or triple exponential decays. One obvious origin of these multi exponential decays is the existence of multiple protein conformations. Since the electric field generated by the nearby amino acids on the indole chromophore depends on the conformation, one expects that the electric field will change the indole lifetime, as will be shown in the following. Although a direct relationship between the emission wavelength and the lifetime cannot be established,[18] it is often observed that a longer lifetime corresponds to proteins emitting at longer wavelength.[19]

 DOI: 10.1039/b308866a

This effect is seen in many proteins like annexinV, or human parathyroidhormone (hPTH), but it is not always the case as in phosphofructokinase (Bs-PFK), for instance.[1]

Considering the success of the Stark effect model to explain the variation of the emission wavelength with the environment, and following the same direction, we are presenting here the results of a theoretical study on the effect of an external electric field on the electronic excited states of indole that probably provide a key mechanism determining the lifetime of Trp in a protein. Indeed, a very recent publication by Callis and Vivian[20] has outlined the role of charge-transfer states for understanding the variation of the Trp lifetime. They consider the charge transfer to the amino group of the peptide chain. Our previous calculations have shown that the $^1\pi\sigma^*$ state is a charge-transfer state with the σ orbital expanding into the space outside the ring, thus this state should be sensitive to interaction with the peptide chain.

The proposal that we are developing here is a consequence of the more general model presented in a recent publication[21] where a surprisingly simple and general mechanistic picture of the non-radiative decay of biomolecules such as nucleic acid bases and aromatic amino acids has been suggested. The key role in this analysis is played by an excited singlet state of $\pi\sigma^*$ character, which has a repulsive potential-energy function with respect to the stretching of OH or NH bonds. The $^1\pi\sigma^*$ potential-energy function intersects not only the bound potential-energy functions of the $^1\pi\pi^*$ excited states, but also that of the electronic ground state (*cf.* Fig. 1 reproduced from ref. 21). These symmetry-forbidden intersections for the planar system are converted into conical intersections when out-of-plane modes are taken into account.[22] The $^1\pi\sigma^*$ state triggers an internal-conversion (IC) process *via* predissociation of the $^1\pi\pi^*$ states and a conical intersection with the ground state. The lifetime of the optically excited $^1\pi\pi^*$ state is thus governed by the first intersection which determines the barrier for IC process, and varies from one molecule to the other depending largely on the energy gap between the $^1\pi\sigma^*$ and the $^1\pi\pi^*$ states.

This model has been already substantiated by several *ab-initio* calculations and agrees well with experimental observations.

(i) In pyrrole[23] (Fig. 1(c)), the $^1\pi\sigma^*$ state is lower than the $^1\pi\pi^*$ and its UV excitation leads to the appearance of hydrogen atoms with a narrow kinetic energy distribution.[24,25] This effect can be related to the direct population of the repulsive $^1\pi\sigma^*$ state.

(ii) In clusters of phenol and ammonia, PhOH–$(NH_3)_n$, calculations predict that the H transfer leads to formation of hydrogenated ammonia clusters $NH_4(NH_3)_n$ through an avoided crossing between the $^1\pi\pi^*$ and the $^1\pi\sigma^*$ states.[26] In contrast to what had been expected,[27–29] the excited state dynamics is not controlled by an excited state proton transfer, but by a hydrogen atom transfer process.[30, 31] In this system the reaction seems to proceed *via* tunneling since the process is fast in the hydrogenated species and considerably slower for deuterated species.[32–34]

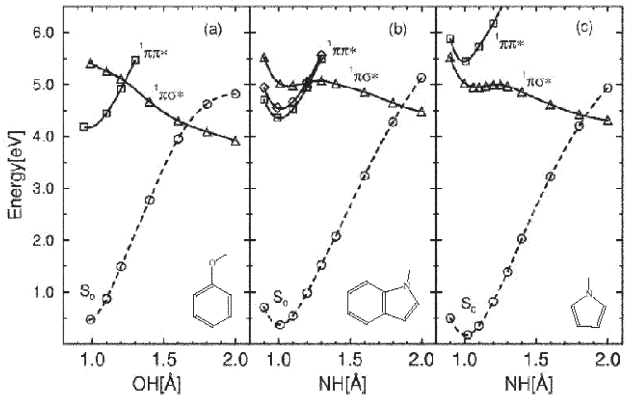

Fig. 1 Potential energy profiles of the lowest $^1\pi\pi^*$ states (□ and ◇), the lowest $^1\pi\sigma^*$ state (△) and the electronic ground state (○) as a function of the OH stretch (phenol) or NH stretch (indole, pyrrole) reaction coordinate. Geometries have been optimized in the excited electronic states at the CASSCF level; the PE profiles have been obtained with the CASMP2 method. Taken from Ref. 21.

(iii) Although less studied, theoretical calculations on the excited states of indole predict an efficient H transfer in the clusters and indeed, excitation of indole–$(NH_3)_n$ (and 3-methylindole–$(NH_3)_n$) clusters leads to the formation of $NH_4(NH_3)_n$ clusters.[14,29] Within an excess of few tenth of eV the reaction proceeds very rapidly, and operates in the 50 ps regime.[15]

(iv) It has been shown, in good agreement with this mechanism, that H atoms are produced when tryptophan is irradiated with ultraviolet light within a protein.[35]

(v) Our model predicts the formation of hydrated electrons as transient species in the H-transfer reaction in aqueous environment. This effect has been observed for numerous aromatic chromophores upon UV excitation in water[36] and indole and Trp are among the best known examples.[6,12]

(vi) The lifetime of 2,3-dimethylindole, measured in a supersonic jet,[8,10] decreases as the excitation energy increases for the hydrogenated species, while for the deuterated molecule (2,3-dimethylindole-d_1) the variation is smaller. This was interpreted as the evidence of a tunneling from the emitting L_b state to the dissociative L_a state. The barrier was assumed to be high enough so only hydrogen atom can tunnel effectively in a time comparable to the radiative lifetime, but deuterium cannot. The recent calculations indicate, however, that the L_a state is not dissociative along the NH stretching coordinate, but that $\pi\sigma^*$ is, and the S_1 lifetime is governed by tunneling through the $^1\pi\pi^*/^1\pi\sigma^*$ avoided crossing.[17]

(vii) In a recent publication Dian *et al.*[37] have shown through combined UV and IR excitation that the indolic NH stretching vibration can easily be observed in the ground state, but not in S_1. This observation is particularly striking in the case of *N*-acetyltryptophan amide (NATA) and *N*-acetyltryptophan methylamide (NATMA) where the NH stretching vibration of the peptide amino group is observed in both the ground and excited state, but the indolic NH-stretch vibration is only observed in the ground state. This can readily be understood presuming a strong coupling between the optically prepared bound $^1\pi\pi^*$ state and the dissociative $\pi\sigma^*$ state along the coordinate of the indolic NH vibration.

In previous calculations on indole, *cf.* Fig. 1(b) and Table 1, it has been shown that the $^1\pi\sigma^*$ state is expected to lie between 0.75 eV[17,38] and 0.42 eV[39] above the L_b ($\pi\pi^*$) state at the ground-state equilibrium geometry (NH distance of about 1 Å). The $^1\pi\sigma^*$ state, which is purely repulsive along the NH bond, crosses the $^1\pi\pi^*$ (L_b and L_a) states at a NH distance of about 1.2 Å. The tunneling through this crossing is expected to control the lifetime of the excited state. The $^1\pi\sigma^*$ state further crosses the ground state at a NH distance of 1.8 Å. The second crossing is responsible for efficient internal conversion to the ground state.

If a nearby molecule is linked to indole by a hydrogen bound involving the H atom of the azine NH group, this hydrogen atom is transferred to the molecule and this process removes the conical intersection with the ground state along the NH stretching coordinate.[26] Then, in an aqueous environment, hydrated electrons can be formed as transient species.[40,41] Under some circumstances, this process can quench the indole (or Trp) fluorescence on the femtosecond time scale, as it will be discussed below.

The $^1\pi\sigma^*$ state is strongly polar at the ground state equilibrium geometry. It has a dipole moment of nearly 10 Debye due to an electron transfer from the ring to the hydrogen atom of the NH bond.[17,39] The dipole moment of the $^1\pi\sigma^*$ state

points in the opposite direction to the dipole moments of the L_a and L_b states (*cf.* Fig. 2). Thus, an electric field produced by the environment on the indole chromophore is expected to modify drastically the $\pi\sigma^*$–$\pi\pi^*$ energy gap. When the splitting is large (~0.5 eV), as estimated for the free molecule (Table 1), a long lifetime is expected,[8,11] whereas the lifetime should be in the femtosecond regime due to a strong $\pi\pi^*/\pi\sigma^*$ mixing and a fast decay along the NH reaction coordinate, if the splitting vanishes.

In the following we present results of calculations on the modifications induced by an electric field on the $\pi\sigma^*$–$\pi\pi^*$ energy gap in indole.

2 Quantum chemical calculations

2.1 Computational methods

The geometry of the ground state and of the three lowest excited singlet states of indole was optimized with the aid of the complete-active-space self-consistent-field (CASSCF) method.[42] The standard Dunning correlation-consistent basis set augmented with polarization and diffuse functions on all atoms (aug-cc-pVDZ)[43] was used in geometry optimization. The active space for the CASSCF calculations for the ground state and for the L_a and L_b $\pi\pi^*$ excited singlet states includes all valence π orbitals. The active space thus correlates 10 electrons in 9 orbitals. For the lowest $\pi\sigma^*$ excited singlet state, this active space was enlarged by including the lowest σ^* orbital. The geometry optimizations were performed with the GAMESS package,[44] and the planar geometry was assumed.

To incorporate electron-correlation effects, single-point calculations at the optimized geometry were performed with the multi-reference second-order Møller–Plesset perturbation theory with respect to the CASSCF reference (CASMP2).[45] The aug-cc-pVDZ basis set used in the CASSCF geometry optimization is diffuse enough for the proper description of the Rydberg-type $\pi\sigma^*$ state in isolated molecule, but to account for the external electric-field effect, this basis set was additionally augmented with a set of diffuse sp functions of exponent 0.02 positioned in the middle of the ring-shared CC bond in the CASMP2 calculations.

The effect of the external electric field on the excited-state CASMP2 energy was calculated as implemented in GAMESS. Namely, the molecule is placed in the xy plane with the ring-shared CC bond along the x axis and the nitrogen atom in the first quarter of the plane (Fig. 2), andthe electric dipole field of a given value and direction was added in the CASMP2 calculation. In this preliminary study, we report the effect of the applied electric field along the Cartesian *x* and *y* axis, *i.e.* parallel to the molecular plane. Our attempt to obtain the CASMP2 energies for the *z* component of the field (perpendicular to the molecular plane) was unsuccessful. The possible reasons of this are discussed below.

When the electric field is applied in the *x* and *y* direction, the symmetry plane is conserved, so that the $\pi\pi^*$ (L_a and L_b) and the $\pi\sigma^*$ excited singlet states belong to different symmetry (A′ and A″, respectively) in the C_s point group. The CASMP2 calculations were thus performed for the state-averaged CASSCF wave functions of the L_a and L_b states and for the single $\pi\sigma^*$ state. The electric-field calculations were performed for each of the optimized geometries including the ground state which served as the reference for the excitation energy. The electronic nature of the states was identified by analysis of the respective CASSCF wave functions. It has turned out that each of the $\pi\pi^*$ states (L_a or L_b) was the lowest excited singlet state at its optimal geometry.

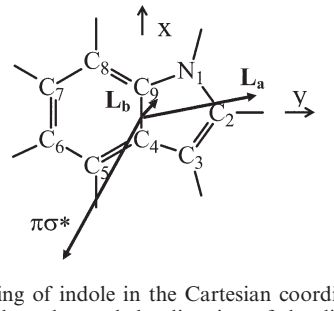

Fig. 2 Positioning of indole in the Cartesian coordinates. The bold arrows indicate the value and the direction of the dipole moment in the different excited singlet states.

When the electric field is applied along the *z* axis, the symmetry plane is broken and all the states belong to the same symmetry block. Thus, the CASMP2 calculations for the *z* component of the field have to be performed for the state-averaged CASSCF wave function including all the excited states of interest. The presence of the diffuse functions in the basis set results in some problems in the CASSCF calculations with external field perpendicular to the molecular ring. Breaking the symmetry plane causes a substantial mixing between π and σ orbitals and the assignment of the states is less certain as compared to the C_s symmetry case. Additionally, the applied field causes a somewhat uncontrolled rotation between orbitals of the active space and orbitals of diffuse Rydberg character which are outside the active space but are stabilized by the external electric field. It turns out that some additional Rydberg-type states are present in the state-averaged CASSCF solution between the valence L_a and L_b states. These effects strongly decrease the credibility of the CASMP2 results obtained in this case, which will not be presented in this paper. Instead, in the following we present results obtained with the aid of the time-dependent density-functional-theory (TDDFT) method.

The TDDFT method,[46] although more approximate than CASMP2, offers some attractive features. Namely, it is less limited with respect to the size of the system, several excited states are obtained in a single calculation, and the assignment of the states is more straightforward than for the state-averaged CASMP2 calculations. Thus a direct comparison between CASMP2 and TDDFT results may have important implications with respect to application of the latter method to large molecular systems of biological relevance. The TDDFT calculations with the B3LYP functional were performed at the same geometries and with the same basis set as CASMP2 calculations discussed above. Additionally, we performed TDDFT calculations at the ground-state equilibrium geometry to check the consequence of geometry changes on the behavior of the excited-state PE surfaces upon an external electric field. The effect of external electric field on the excited-state TDDFT energies was calculated as implemented in Gaussian 98 program package.[47]

2.2 Results

2.2.1 Geometric and electronic structures. The ground state, two low-lying valence $\pi\pi^*$ and the lowest Rydberg-type $\pi\sigma^*$ excited singlet states were optimized at the CASSCF level of theory, as described in the previous section. The resulting geometry parameters are presented in Table 1. For the ground and the lowest valence L_b states, the results of Serrano-Andrés and Roos[39] are reproduced to a significant extent. The difference in bond lengths and bond angles is generally of the order of 0.001 Å and 0.1°, respectively. The L_a state is exceptional with this respect, and the geometry determined in this work differs remarkably with respect to results of ref. 39. Variation of bond lengths and bond angles as large as 0.05 Å and 1.0°, respectively, can be noticed. Let us to mention that, for this L_a state, a similar scatter of results obtained with the aid of different theoretical methods has been collected in ref. 39. In our opinion, this effect can be explained as follows. The equilibrium

Table 1 Bond lengths and bond angles optimized with the CASSCF method for the ground state and for the three lowest excited states of indole (see Fig. 2 for enumeration of atoms)

Bond	S_0	$L_b(\pi\pi^*)$	$L_a(\pi\pi^*)$	$\pi\sigma^*$	Angle	S_0	$L_b(\pi\pi^*)$	$L_a(\pi\pi^*)$	$\pi\sigma^*$
N_1C_2	1.378	1.391	1.313	1.297	$N_1C_2C_3$	109.7	108.8	106.7	109.6
C_2C_3	1.367	1.383	1.435	1.452	$C_2C_3C_4$	106.7	107.7	107.5	106.1
C_3C_4	1.444	1.427	1.468	1.410	$C_3C_4C_5$	134.0	134.0	133.1	134.1
C_4C_5	1.410	1.419	1.411	1.412	$C_4C_5C_6$	118.9	117.8	115.1	118.1
C_5C_6	1.387	1.444	1.431	1.397	$C_5C_6C_7$	120.9	121.7	123.4	121.2
C_6C_7	1.415	1.440	1.365	1.404	$C_6C_7C_8$	121.2	120.9	122.0	121.6
C_7C_8	1.388	1.433	1.446	1.416	$C_7C_8C_9$	117.6	116.9	113.0	116.4
C_8C_9	1.405	1.412	1.404	1.374	C_9N_1H	125.6	124.8	123.6	126.4
N_1H	0.995	0.995	1.003	1.029	N_1C_2H	120.6	120.9	122.7	121.0
C_2H	1.077	1.075	1.076	1.078	C_2C_3H	126.0	125.5	124.6	125.0
C_3H	1.077	1.078	1.077	1.077	C_4C_5H	120.5	119.3	122.6	120.8
C_5H	1.082	1.079	1.078	1.080	C_5C_6H	119.9	119.3	118.2	119.6
C_6H	1.082	1.080	1.084	1.080	C_6C_7H	119.3	119.2	119.3	119.5
C_7H	1.082	1.080	1.082	1.080	C_7C_8H	121.0	121.2	123.4	121.7
C_8H	1.082	1.080	1.078	1.078					

geometry of the L_b state represents a global minimum on the excited singlet state PE surface and is well separated from the next excited singlet state (CASSCF energy of the L_a state at the L_b geometry is by 1.36 eV higher). On the other hand, the equilibrium geometry of the L_a state represents a local minimum, and the vertical CASSCF energy of the L_b state at this geometry is only 0.22 eV above. These states are thus expected to be subject to strong vibronic interactions with each other. Since both L_a and L_b states belong to the same totally symmetric representation of the C_s point group, the in-plane vibrational modes are involved into the coupling. An energy gap of 0.22 eV is of the order of a typical vibrational frequency of the skeletal stretching and bending modes thus the PE landscape along these modes is expected to be most strongly influenced by the vibronic interactions. Since the energy gap between the L_a and L_b states depends on the theoretical method and the basis set used in the calculation, a large variation of geometry of the L_a state is determined in different works (see ref. 39, and references therein).

The geometry of the Rydberg-type $\pi\sigma^*$ state was for the first time obtained at this level of theory, so the comparison to other works is not possible. Inspection of the results presented in Table 1 shows that the most important changes of geometry for the $\pi\sigma^*$ state with respect to the ground state involve increase of the double bond lengths and decrease of the single bond lengths. This behavior is related to the transfer of electron from the aromatic ring (π orbital) to the σ^* orbital localized mostly on the NH moiety as discussed in ref. 17.

The CASMP2 and TDDFT excitation energies for the lowest singlet states are shown in Table 2. They were calculated at the equilibrium geometry of the respective states thus, apart from the zero-energy corrections, they represent adiabatic excitation energies. The vertical transition energies (obtained at the ground-state geometry) are also given for comparison. Our CASMP2 results for the lowest $\pi\pi^*$ states are in reasonably good agreement with the results of Serrano-Andrés and Roos[39] obtained with a similar theoretical method (CASPT2), but with different basis set and at slightly different geometries. Both the CASMP2 and the CASPT2 results reproduce experimental observations (*cf.* results collected in ref. 39) within the expected precision of these theoretical methods, although the L_b state seems to be remarkably underestimated by the CASMP2 method. The experimental energy of the $\pi\sigma^*$ Rydberg-type state is unknown at present because this state is essentially ''dark'' for direct absorption from the ground state (its theoretically estimated oscillator strength is between 10^{-3} [39] and 10^{-5} [17]) and is embedded within the ro-vibrational manifold of the lower-lying $\pi\pi^*$ states. The vertical energy of the $\pi\sigma^*$ state obtained in this work is in good agreement with the vertical energy reported in ref. 39 (Table 2), and its adiabatic energy is lower by about 0.4 eV. This is a similar amount of energy as found from comparison of adiabatic and vertical energies of the $\pi\pi^*$ states.

The TDDFT results presented in Table 2 show that although the relative location of the L_a and $\pi\sigma^*$ states is very similar to the CASMP2 result, the TDDFT energy of the L_b state is the highest among the three excited states considered in this work. The difference between the adiabatic energy of the L_b state predicted by the two theoretical methods is as large as 0.67 eV. This discrepancy can be related to the different approximations involved into the two theoretical methods. Apparently, two-electronic and higher excitations which are largely ignored by the TDDFT method are relatively more important for the L_b state than for the L_a state. Inclusion of this effect at the variational CASSCF level is thus crucial for the proper ordering of these states.

The distinct spectroscopic properties of the lowest excited states of indole are reflected by differences in their wave functions and the resulting dipole moment of each electronic state (Fig. 2). The CASSCF dipole moments of the ground state (1.96 D), of the L_b (1.62 D) and the L_a (7.82 D) excited states, determined at the respective equilibrium geometries, are in reasonably good agreement with experimental values (2.09 D,[48] 2.3 D[49] and 5.7 D[50]), as well as with other theoretical data.[17,39] Although, the L_a state is significantly more polar than the L_b state and the ground state, the dipole moments of these states are aligned in the first quarter of the molecular plane as illustrated in Fig. 2. The $\pi\sigma^*$ Rydberg-type state is much more polar than the valence states with a dipole moment of 11.09 D which is moreover almost perfectly anti-parallel to the dipole moments of the $\pi\pi^*$ states (Fig. 2). It is thus expected that the two most polar states (L_a and $\pi\sigma^*$) of indole will respond in a different way to the applied external electric field. The TDDFT method as it is implemented in Gaussian 98 does not allow to calculate the excited states dipole

Table 2 Theoretical and experimental energies of the three lowest excited singlet states of indole

State	CASMP2[a]	TD-B3LYP[a]	CASPT2[b]	experiment[d]
$L_b(\pi\pi^*)$	4.05 (4.55)	4.83 (4.92)	4.35	4.37
$L_a(\pi\pi^*)$	4.45 (4.96)	4.56 (4.79)	4.67	4.54
$\pi\sigma^*$	4.67 (5.08)	4.66 (4.72)	4.85[c]	–

[a] Adiabatic and vertical (in parentheses) energy of this work. [b] Adiabatic energy of ref. 39. [c] Vertical energy of ref. 39. [d] Adiabatic energy ref. 16.

moments, so comparison between the methods in this respect is not possible.

2.2.2 Electric field effect. The evolution of the CASMP2 adiabatic energy of the lowest excited singlet states of indole as a function of the external electric field applied along the x and y Cartesian coordinates is presented in the upper part of Fig. 3. The respective TDDFT results are given for comparison in the lower part of the figure.

Before discussing the results shown in Fig. 3, lets us comment a technical detail related to the construction of this figure. Although, with some exceptions, the theoretical energies of the excited states of interest are reasonably close to experimental values, we decided to show also the CASMP2 adiabatic energy of the L_b and L_a states and the TDDFT of the L_b state at $E = 0$ (no external field applied) adjusted to experimentally observed position of the 0–0 line of a given electronic transition in order to account for subtle resonant effect which can be caused by the external field. This means that the CASMP2 energy of the L_b and L_a states were risen by 0.32 and 0.09 eV, respectively, while the TDDFT adiabatic energy of the L_b state was shifted down by 0.46 eV in order to reproduce the correct ordering of the states. The TDDFT energy of the L_a , as well as both CASMP2 and TDDFT adiabatic energies of the $\pi\sigma^*$ state were left at the calculated values in view of marginally small difference with respect to experiment (L_a state) or to other theoretical values ($\pi\sigma^*$ state). The corrected CASMP2 potential energy functions of the L_b and L_a states (Fig. 3(a) and (b)) and corrected TDDFT potential energy function of the L_b state (Fig. 3(c) and (d)) are represented by dashed lines.

The results shown in Fig. 3(a) and (b), indicate a relatively small variation of the L_b state within the range of the applied external electric field, as expected from the small dipole moment of this state, *cf.* Fig. 2. On the other hand, both polar states, L_a and $\pi\sigma^*$, show a remarkable modulation of their energy upon the applied field. These states cross each other at relatively small positive value of the electric field applied either along the x or y direction. For larger negative value of the field (E_x or E_y), the L_a state crosses the L_b state and becomes the lowest excited singlet state of the system. Since the L_a state is "allowed" for absorption from the ground state, alignment of the external electric field along these directions is thus expected to increase the indole fluorescence. If, however, the electric field is aligned along the positive x or y directions, the $\pi\sigma^*$ state is stabilized and becomes the lowest excited singlet state of the system for large values of the field. This alignment of the electric field is thus expected to decrease the fluorescence yield of the system because the $\pi\sigma^*$ state is almost "forbidden" for absorption from the ground state, and is supposed to induce an efficient radiationless decay related to the detachment of the hydrogen atom from the NH group.[17]

The TDDFT results presented in Fig. 3(c) and (d), are qualitatively similar to the respective CASMP2 results with a noticeable exception for the L_a state when the field is applied along the short molecular axis x. Whereas there is a strong variation of the L_a state energy in response to the E_x component of the field at the CASMP2 level (Fig. 3(a)), the TDDFT energy is almost invariant (like the L_b state) with the strength of the field applied in this direction. This could be understandable if the L_a TDDFT dipole moment was aligned along the long molecular axis y, with no component along the short molecular axis x. Unfortunately, the TDDFT method in its current implementation with Gaussian does not allow to calculate the excited states dipole moments.

We want to stress that the level crossings visible in Fig. 3 are not real crossings, because all the states are calculated at their equilibrium geometry. These are thus apparent crossings resulting from one-dimensional projection of the multi-dimensional PE surfaces. To illustrate the effect of real crossings between the PE functions of the excited singlet states caused by the external electric field, we present the variation of TDDFT vertical energies obtained at the ground state geometry in Fig. 4. To get the proper ordering of the states we shifted down TDDFT vertical energy of the L_b state by 0.37 eV to reproduce the vertical CASMP2 energy of this state at $E = 0$ (Table 2) as discussed above (dashed line with squares in Fig. 4). In the same way, the TDDFT vertical energy of the $\pi\sigma^*$ state was shifted up by 0.4 eV (Table 2) to reproduce the vertical CASMP2 energy at $E = 0$ (dashed line with triangles in Fig. 4).

The results presented in Fig. 4(a) and (b) are qualitatively similar to the adiabatic PE functions shown in Fig. 3(c) and (d), but now the crossing between the $\pi\pi^*$ and $\pi\sigma^*$ states are real, because they are calculated at the same ground state geometry. Thus an external electric field of sufficient strength is able to change the ordering of the lowest excited singlet states of indole.

The electric field applied along the x or y axis modulates the energy gap between the $\pi\sigma^*$ and $\pi\pi^*$ states, but does not induce any coupling between them, because the planar C_s symmetry is preserved. When the external field is applied

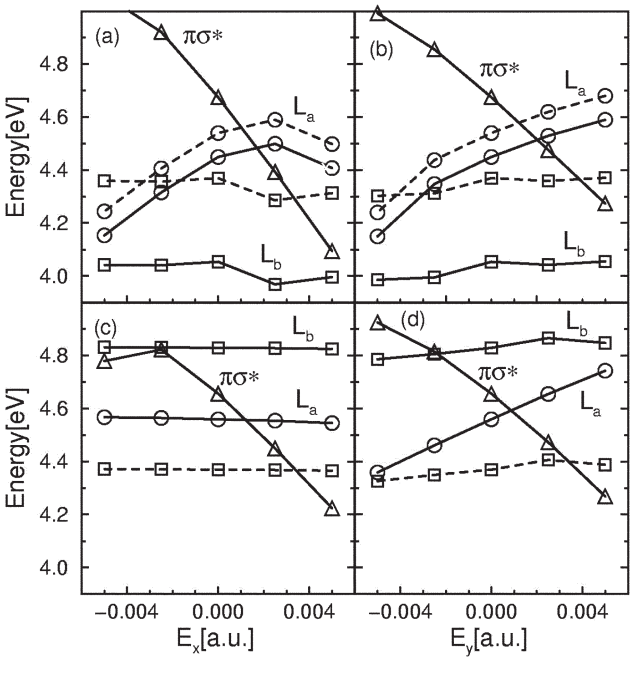

Fig. 3 Variation of the CASMP2 (upper panels) and TDDFT (lower panels) adiabatic energies of the lowest excited singlet states: L_b (□), L_a (○) and $\pi\sigma^*$ (△), as a function of the external electric field applied along the x- (a and c) and y- (b and d) Cartesian axis. The dashed lines represent the energies normalized at $E = 0$ to the experimental 0–0 line, respectively, for the L_a and L_b states.

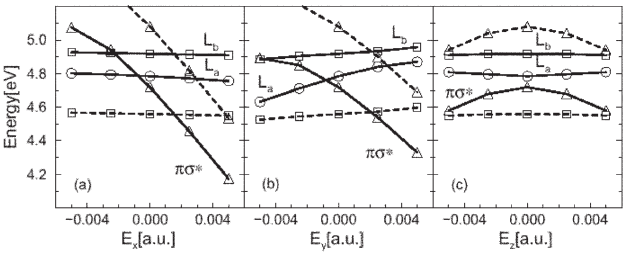

Fig. 4 Variation of the TDDFT vertical energies of the lowest excited singlet states: L_b (□), L_a (○) and $\pi\sigma^*$ (△), as a function of the external electric field applied along the x- (a), the y- (b) and the z- (c) Cartesian axis. The dashed lines represents the TDDFT energy of the L_b and $\pi\sigma^*$ states normalized to the CASMP2 vertical energy of these states, respectively, at $E = 0$.

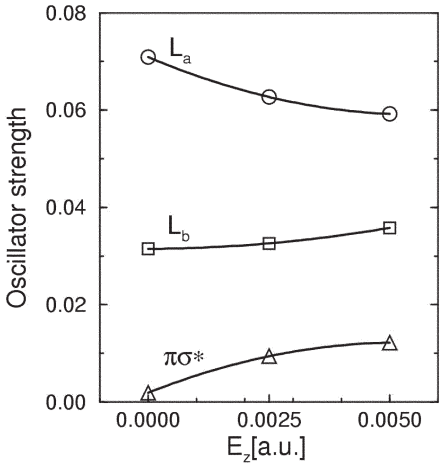

Fig. 5 Variation of the oscillator strength of the lowest excited states as a function of the external electric field applied along the z Cartesian axis. L_b (□), L_a (○) and πσ* (△).

perpendicularly to the molecular plane, the C_s symmetry of the Hamiltonian of the system is broken and the coupling between the πσ* and ππ* states is turned on. The effect of the E_z component of the electric field on the vertical TDDFT energies of the states is shown in Fig. 4(c). Once again, the energy of the L_b state is almost independent of the applied field, but both the L_a and πσ* more polar states respond remarkably to the E_z field, although their dipole moments are in-plane polarized. What is clearly visible from Fig. 4(c) is an apparent repulsion between L_a and πσ* states induced by the external field. Analysis of the relevant molecular orbitals and CI coefficients of the TDDFT wave functions shows that there is a substantial mixing between all the excited states. This effect can transparently be visualized by examination of the oscillator strengths for absorption from the ground state to the respective excited singlet states shown in Fig. 5.

The πσ* state which is essentially "dark" for absorption from the ground state for $E = 0$ ($f = 0.002$) gains remarkable intensity ($f = 0.012$) at $E_z = 0.005$ a.u. The intensity borrowing is at the expense of a decrease in oscillator strength for the "allowed" absorption to the L_a state ($f = 0.071$ at $E = 0$ down to $f = 0.059$ at $E_z = 0.005$ a.u.). A perpendicular electric field also amplifies the coupling between the L_a and L_b states as can be seen from variation of oscillator strength of the latter state.

Although we were unable to get converged CASMP2 results for the E_z component of the external field, the qualitative agreement between the TDDFT and CASMP2 PE profiles obtained for a field aligned along the x or y axis, as discussed above, allows us to conclude that this is also the case for perpendicular alignment of the field. Thus, an important effect of the perpendicular electric field, apart from the modulation of the ππ*–πσ* energy gap, is a more effective coupling of the ππ* manifold to the non radiative decay channels provided by the πσ* state.

3 Molecular dynamic simulation and discussion

The calculations presented above show that the electric field induced by the environment on the indole chromophore of tryptophan can produce a significant modulation of the ππ*–πσ* energy gap, which governs an access to the non radiative decay channels of the S_1 state of indole. Some aspects of this effect have to be discussed.

3.1 Order of magnitude of the electric field

The calculations have indicated that the magnitude of the external electric field on the indole molecule should be in the range of $2–5 \times 10^{-3}$ a.u. to induce a noticeable effect on the ππ*–πσ* energy gap. In order to estimate the strength of the electric field experienced by indole in a protein, we have calculated the field induced on the indole chromophore of a small protein (Cobra toxin) in an environment of 840 water molecules using molecular dynamics simulations with the Amber force field. The histogram of the electric field intensity fluctuations along the x, y and z coordinates, calculated at the origin of the coordinates (in the middle of the ring-shared CC bond, Fig. 2) during a trajectory run at 300 K, is presented in Fig. 6. This calculation takes into account the partial charges of the 840 water molecules around the protein and all the atoms which do not belong to the indole rings. The histogram shows that, at this temperature, the magnitude of the field is varying considerably up to 5×10^{-3} a.u., and for instance the mean value for the E_x component is -3.2×10^{-3} a.u.. The field values obtained in this simulation are thus large enough to cause a significant modulation of the ππ*–πσ* energy gap which may eventually lead to an intersection between the states as discussed in the previous section.

3.2 ππ*–πσ* energy gap and excited state lifetime

This paper deals only with the ππ*–πσ* energy gap modulation induced on the indole chromophore of tryptophan by the electric field induced by the environment. The link between the energy gap and the excited state lifetime remains to be established, but some guidelines can be drawn. When $E_z = 0$, the planar symmetry is preserved, and the decay of the ππ* state is mediated by its conical intersection with the πσ* state. A

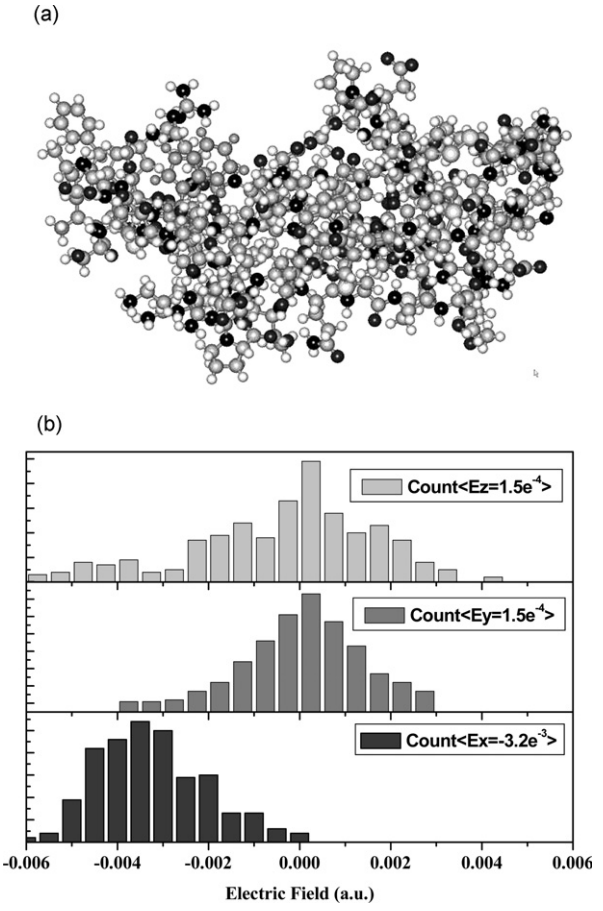

Fig. 6 Top: Alpha cobra-toxin protein taken from the Protein Data Bank (1CTX in PdB nomenclature). This protein contains only one tryptophan residue. Bottom: calculated electric field induced along the x,y,z Cartesian axis at the middle of the indole chromophore by the rest of the protein surrounded by 840 water molecules. The mean value of the E_x field is -3.2×10^{-3} a.u.

smaller energy gap will clearly decrease the $\pi\pi^*$ S_1 lifetime, just by lowering the intersection seam. In this case, out-of-plane molecular vibrations induce the internal conversion process. When E_z is non-zero, the C_s symmetry of the electronic Hamiltonian is broken and the $\pi\pi^*$ and $\pi\sigma^*$ states are mixed, as discussed previously, even for the planar arrangement of nuclei. In this case, the lifetime is not only affected by the location of the intersection, but also by the degree of mixing.

In any case, the $\pi\pi^* \rightarrow \pi\sigma^*$ non adiabatic transition can be viewed as a tunneling across the conical intersection, along the NH coordinate. The tunneling probability depends strongly on the barrier height and on its width, but quantitative characterization of the barrier at the excited state PE surfaces with the nowadays-available quantum chemical methods is still far from the precision desired.

3.3 Correlation between longer lifetime and red shift

As mentioned in the introduction, a correlation between the red shift of the tryptophan fluorescence in proteins and a longer lifetime is often found, although this correlation is far from being perfect. In the weak electric field limit ($|E| < 0.0025$ a.u.), in particular when the field is applied along the y axis (Fig. 3(b)), the energy gap between the emitting L_a state and the ground state decreases and this corresponds to a red shifted fluorescence. Eventually, for a larger negative value of the field applied in a molecular plane, the emitting L_a state can become the lowest excited singlet state of the system, thus further increasing the fluorescent properties of the system. Under the same conditions, the L_a–$\pi\sigma^*$ energy gap increases, thus the barrier for internal conversion gets higher and a longer fluorescence lifetime is expected.

3.4 Hydrogen bonding

In the representation described above, only the free indole chromophore has been considered. In the condensed phase, indole is often linked to another molecule (solvent or amino acid residue) by hydrogen bonding, which is expected to influence strongly the $\pi\pi^*/\pi\sigma^*$ coupling. Two limiting cases can be discussed, depending on the ''hydrogen affinity'' of the molecule bound to the indolic NH moiety. If the molecule bound to indole has a strong hydrogen affinity, like ammonia, the departing H atom can be captured by the nearby molecule leading to the formation of hydrogenated radicals such as the ammonium radical NH_4, and the lifetime of the indole excited state will be reduced. On the other hand, if the hydrogen affinity of the hydrogen bonded molecule is poor (as for water), the $\pi\sigma^*$ state is pushed up at intermediate NH distance, the $\pi\pi^*/\pi\sigma^*$ crossing occurs at a higher energy and therefore the lifetime increases. Such effects have been very well characterized in the case of phenol clusters.[26,29] In phenol–$(NH_3)_n$ clusters, excitation to S_1 leads to the formation of $NH_4(NH_3)_n$ clusters, and the S_1 lifetime is shortened (1 ns for the phenol–NH_3 complex, 400 ps for phenol–$(NH_3)_2$). On the other hand, the lifetime of phenol–H_2O (16 ns) is longer than that of the free phenol (2 ns).[51] A similar behavior has been recorded for 3-methylindole where the lifetime of the ammonia complex is very short as compared to that of the water complex.[8,11] The hydrogen affinity concept which corresponds to the possibility for a solvent molecule to capture the departing H atom and to produce a (meta)stable radical, just begins to be characterized for some simple neutral solvent molecules such as H_2O[40,52] and NH_3,[53,54] and will require more experimental and theoretical work.

3.5 Solvated electrons and fluctuations of the electric field

At first glance, it seems difficult to reconcile two experimental observations: the lifetime of indole in water is in the order of 4.4 ns[1,55] after excitation of the $\pi\pi^*$ state, but hydrated electrons are produced in less than 100 fs[12] after excitation of indole in the 266 nm energy range, although the quantum yield for this process is very small.

This behavior can be understood with our model in taking into account the following arguments to run molecular dynamics simulations.

(i) When the $\pi\sigma^*$ state of an aromatic chromophore is populated, an electron is ejected to the aqueous solvent (charge-transfer to the solvent, CTTS, process) as shown by previous *ab initio* calculations.[23,26,38] The electron ejection is followed by proton transfer (PTTS) leading in fact to a hydrogen transfer (HTTS) process and to the formation of hydronium radical (H_3O).

(ii) The hydronium radical solvated in water has been found to be a charge-separated complex, consisting of a hydronium cation and a 'solvated' electron cloud.[40,41] Its characteristic spectroscopic features (calculated VIS and IR absorption spectra)[40,56,57] have lead to the conclusion that the solvated hydronium radical is a precursor of the hydrated electron.

(iii) However, it seems difficult to reach the $\pi\sigma^*$ state with a 266 nm (4.66 eV) excitation of the free molecule, since this state lies above 4.8 eV and its oscillator strength is too small for effective one-photon excitation. In order to be optically accessible the $\pi\sigma^*$ has to be lower in energy and to mix efficiently with the ''allowed'' L_a state. The results presented above show that the $\pi\sigma^*$ state energy strongly depends on the local electric field, and can be drastically influenced by fluctuations of the environment.

Whether an environment of water around the indole molecule can generate an electric field strong enough to mix the $\pi\pi^*$ and $\pi\sigma^*$ states can be tested in running classical trajectories involving one indole molecule solvated by 512 water molecules at 300 K using the Amber force field. The results are shown in Fig. 7. The calculated fluctuations of the electric

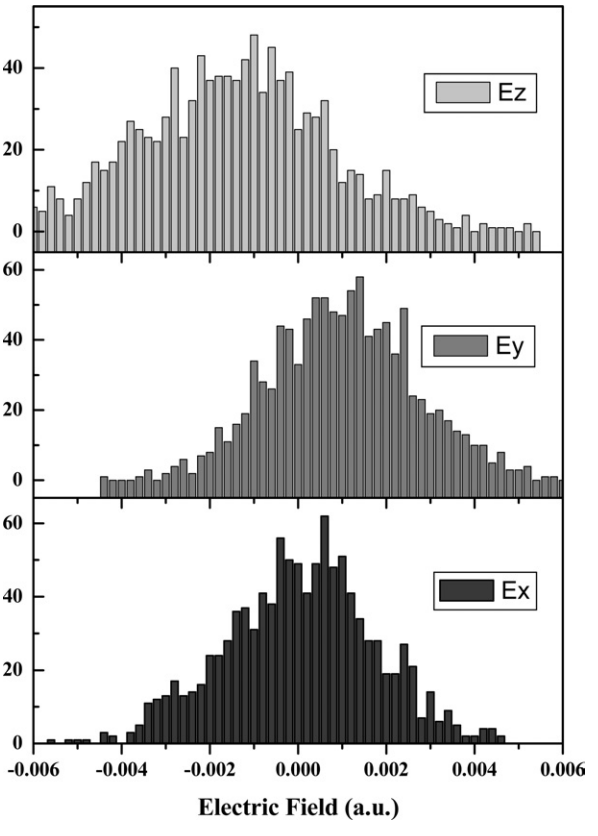

Fig. 7 Histogram of the electric field fluctuations induced by 512 water molecules surrounding an indole molecule at 300 K. The trajectory has been run for 1.5 ps but because the system must equilibrate, the first 0.5 ps are not taken into account. The electric field is calculated every 20 fs while the integration step is 1 fs.

field are surprisingly large and particularly so along the z axis, so that the indole spends some time in an environment with a local E_z field strong enough to mix the ππ* and πσ* states.

Keeping these points in mind, the detection of solvated electrons produced at the sub-picosecond time scale and the nanosecond lifetime of the excited state might be understood in the following way:

(i) Some molecules are excited in a local environment where E_z is large enough so that excitation leads to the mixed ππ*/πσ* state that can immediately eject an electron (or a hydrogen atom leading to the formation of a hydronium radical) to the solvent resulting in the observation of "solvated electrons".

(ii) Most of the molecules are in a local environment where the field is smaller than the threshold for interstate mixing. In this case, the ππ* state is excited and since the coupling to the πσ* state is weak, a long (nanosecond) lifetime is observed.

This interpretation would need to be refined; in particular, the time dependent solvent reorganization that occurs after optical excitation should be taken into account and can modify this simple picture.

4 Conclusions and prospects for the future

In this paper, we have pointed out that the energy gap between the ππ* and πσ* lowest excited singlet states of indole is strongly modulated by the local electric field acting on the indole ring. The ππ*–πσ* energy gap, of 0.4–0.6 eV, in the absence of external field, decreases strongly or even vanishes in a moderate electric field of about 5×10^{-3} a.u. Since the lifetime of the emitting ππ* singlet state is governed by the ππ*/πσ* crossing, as demonstrated in many experiments in clusters, this local field effect provides an attractive mechanistic picture for understanding the variations of the tryptophan fluorescence lifetime in proteins.

The present work will be complemented in the following directions:

(i) The results presented in this work shows a qualitative agreement between the CASMP2 and TDDFT methods as far as the response of the excited singlet state energy to the external electric field is concerned, although ordering of the states appears to be sensitive to the theoretical method used.

(ii) A full map of the variation of the ππ*–πσ* energy gap, $\Delta E_{\pi\pi^*/\pi\sigma^*}$, as a function of the three components of the field (E_x, E_y, E_z) has to be established in order to obtain, if possible, an analytical formula $\Delta E_{\pi\pi^*/\pi\sigma^*} = f(E_x, E_y, E_z)$, which will then be used in molecular dynamic simulations of the effect.

(iv) A link between the ππ*–πσ* energy gap and the lifetime of the S_1 state should be established: this might be achieved using simple test systems for which the calculations and experiments can easily be compared.

(v) Finally, the role of a specific environment, in particular hydrogen bonded systems, has to be investigated.

Acknowledgements

This work has been supported by the CNRS - Polish Academy of Sciences exchange program and the Committee for Scientific Research of Poland (Grant No. 3 T09A 082 19).

References

1 J. R. Lakowicz, *Principles of fluorescence spectroscopy*, Kluwer Academic/Plenum Publishers, New York, Boston, Dordrecht, London, Moscow, 2nd edn., 1999.
2 Y. Chen and M. D. Barkley, *Biochemistry*, 1998, **37**, 9976.
3 J. T. Vivian and P. R. Callis, *Biophys. J.*, 2001, **80**, 2093.
4 M. T. Pailthorpe and C. H. Nicholls, *Photochem. Photobiol*, 1971, **14**, 135.
5 A. Z. Britten and G. Lockwood, *Spectrochim. Acta*, 1976, **32**, 1335.
6 J. C. Mialock, E. Amouyal, A. Bernas and D. Grand, *J. Phys. Chem.*, 1982, **86**, 3173.
7 J. W. Petrich, M. C. Chang, D. B. McDonald and G. R. Flemming, *J. Am. Chem. Soc.*, 1982, **105**, 3824.
8 J. W. Hager, D. R. Demmer and C. S. Wallace, *J. Phys. Chem.*, 1987, **91**, 1375.
9 R. J. Lipert, G. Bermudez and S. D. Colson, *J. Phys. Chem.*, 1988, **92**, 380.
10 D. R. Demmer, G. W. Leach, E. A. Outhouse, J. W. Hager and S. C. Wallace, *J. Phys. Chem.*, 1990, **94**, 582.
11 S. Arnold and M. Sulkes, *J. Phys. Chem.*, 1992, **96**, 4768.
12 J. Peon, G. C. Hess, J. M. L. Pecourt, T. Yuzawa and B. Kohler, *J. Phys. Chem. A*, 1999, **103**, 2460.
13 K. W. Short and P. R. Callis, *J. Chem. Phys.*, 2000, **113**, 5235.
14 C. Dedonder-Lardeux, D. Grosswasser, C. Jouvet and S. Martrenchard, *Phys. Chem. Comm*, 2001, 1–3.
15 H. Lippert, V. Stert, L. Hesse, C. P. Schulz, W. Radloff and I. V. Hertel, *Eur. Phys. J. D*, 2002, **20**, 445.
16 B. J. Fender, D. M. Sammeth and P. R. Callis, *Chem. Phys. Lett.*, 1995, **239**, 31.
17 A. L. Sobolewski and W. Domcke, *Chem. Phys. Lett.*, 1999, **315**, 293.
18 M. R. Eftink, *Methods Biochem. Anal.*, 1991, **35**, 127–205.
19 A. Hafner, F. Merola, G. Duportail, R. Hutterer, F. W. Schneider and M. Hof, *Biopolymers*, 2000, **57**, 226–234.
20 P. R. Callis and J. T. Vivian, *Chem. Phys. Lett.*, 2003, **369**.
21 A. L. Sobolewski, W. Domcke, C. Dedonder-Lardeux and C. Jouvet, *Phys. Chem. Chem. Phys.*, 2002, **4**, 1093–1100.
22 A. L. Sobolewski and W. Domcke, *Eur. Phys. J. D*, 2002, **20**, 369.
23 A. L. Sobolewski and W. Domcke, *Chem. Phys. Lett.*, 2000, **321**, 479–484.
24 D. A. Blank, S. W. North and Y. T. Lee, *Chem. Phys.*, 1994, **187**, 35–47.
25 J. Wei, A. Kuczmann, J. Riedel, F. Renth and F. Temps, *Phys. Chem. Chem. Phys.*, 2003, **5**, 315–320.
26 A. L. Sobolewski and W. Domcke, *J. Phys. Chem.*, 2001, **105**, 9275.
27 J. A. Syage and J. Steadman, *J. Chem. Phys.*, 1991, **95**, 2497.
28 D. Solgadi, C. Jouvet and A. Tramer, *J. Phys. Chem.*, 1988, **92**, 3313.
29 O. David, C. Dedonder-Lardeux and C. Jouvet, *Int. Rev. Phys. Chem.*, 2002, **21**, 499.
30 G. Pino, G. Gregoire, C. Dedonder-Lardeux, C. Jouvet, S. Martrenchard and D. Solgadi, *Phys. Chem. Chem. Phys.*, 2000, **2**, 893–900.
31 G. A. Pino, C. Dedonder-Lardeux, G. Gregoire, C. Jouvet, S. Martrenchard and D. Solgadi, *J. Chem. Phys.*, 1999, **111**, 10 747.
32 G. Gregoire, C. Dedonder-Lardeux, C. Jouvet, S. Martrenchard, A. Peremans and D. Solgadi, *J. Phys. Chem. A*, 2000, **104**, 9087–9090.
33 S. Ishiuchi, K. Daigoku, M. Saeki, K. Hashimoto, M. Sakai and M. Fujii, *J. Chem. Phys.*, 2002, **117**, 7083.
34 S. Ishiuchi, K. Daigoku, M. Saeki, K. Hashimoto, M. Sakai and M. Fujii, *J. Chem. Phys.*, 2002, **117**, 7077.
35 P. J. Angiolillo and J. M. Vanderkooi, *Photochem. Photobiol*, 1996, **64**, 492.
36 H. I. Joschek and L. I. Grossweiner, *J. Am. Chem. Soc.*, 1966, **88**, 3261.
37 B. C. Dian, A. Longarte and T. S. Zwier, *J. Chem. Phys.*, 2003, **118**, 2696.
38 A. L. Sobolewski and W. Domcke, *Chem. Phys. Lett.*, 2000, **329**, 130.
39 L. Serrano-Andrés and B. O. Roos, *J. Am. Chem. Soc.*, 1996, **118**, 185.
40 A. L. Sobolewski and W. Domcke, *Phys. Chem. Chem. Phys.*, 2002, **4**, 4.
41 A. L. Sobolewski and W. Domcke, *J. Phys. Chem. A*, 2002, **106**, 4158.
42 B. O. Roos, *Adv. Chem. Phys.*, 1987, **69**, 399.
43 D. E. Woon and T. H. Dunning, Jr., *J. Chem. Phys.*, 1993, **98**, 1358.
44 M. W. Schmidt, K. K. Baldridge, J. A. E. Boatz, S. T. Elbert, M. S. Gordon, J. H. Jensen, S. Koseki, M. Matsunaga, K. A. Nguyen, S. J. Su, T. L. Windus, M. Dupuis and J. A. Montgomery, *J. Comput. Chem.*, 1993, **14**, 1347.
45 J. H. Nakano, *Chem. Phys.*, 1993, **99**, 7983.

46 E. K. U. Gross and W. Kohn, *Adv. Quantum Chem.*, 1990, **21**, 255.
47 M. J. Frisch, G. W. Trucks, H. B. Schlegel, G. E. Scuseria, M. A. Robb, J. R. Cheeseman, V. G. Zakrzewski, J. A. Montgomery, Jr., R. E. Stratmann, J. C. Burant, S. Dapprich, J. M. Millam, A. D. Daniels, K. N. Kudin, M. C. Strain, O. Farkas, J. Tomasi, V. Barone, M. Cossi, R. Cammi, B. Mennucci, C. Pomelli, C. Adamo, S. Clifford, J. Ochterski, G. A. Petersson, P. Y. Ayala, Q. Cui, K. Morokuma, D. K. Malick, A. D. Rabuck, K. Raghavachari, J. B. Foresman, J. Cioslowski, J. V. Ortiz, B. B. Stefanov, G. Liu, A. Liashenko, P. Piskorz, I. Komaromi, R. Gomperts, R. L. Martin, D. J. Fox, T. Keith, M. A. Al-Laham, C. Y. Peng, A. Nanayakkara, C. Gonzalez, M. Challacombe, P. M. W. Gill, B. G. Johnson, W. Chen, M. W. Wong, J. L. Andres, M. Head-Gordon, E. S. Replogle and J. A. Pople, *GAUSSIAN 98*, Gaussian, Inc., Pittsburgh, PA, 1998.
48 W. Caminati and S. Di Bernardo, *J. Mol. Struct.*, 1990, **240**, 253.
49 C. T. Chang, C. Y. Wu, A. R. Muirhead and J. R. Lombardi, *Photochem. Photobiol.*, 1974, **19**, 347.
50 H. Lami and N. J. Glasser, *J. Chem. Phys.*, 1986, **84**, 597.
51 R. J. Lipert and S. D. Colson, *J. Phys. Chem.*, 1990, **94**, 2358.
52 M. Luo and M. Jungen, *Chem. Phys.*, 1999, **241**, 297.
53 K. Daigoku, N. Miura and K. Hashimoto, *Chem. Phys. Lett.*, 2001, **346**, 81.
54 E. Kassab and E. M. Evleth, *J. Am. Chem. Soc.*, 1986, **109**, 1653.
55 M. R. Eftink, Y. Jia, D. Hu and C. A. Ghiron, *J. Phys. Chem.*, 1995, **99**, 5713–5723.
56 F. Muguet, Y. Gauduel and H. Gelabert, *TMMeC Web Journal (The Molecular Modeling Electronic Conference ISSN 0797-9274)*, 1997, vol. 1, issue 2, p. 38.
57 F. Muguet, H. Gelabert and Y. Gauduel, *J. Chim. Phys.*, 1996, **93**, 1808.